universe

IMPACT FACTOR 2.9

CITESCORE 3.6

Article

Dependence of Freeze-Out Parameters on Collision Energies and Cross-Sections

Muhammad Waqas, Atef AbdelKader, Muhammad Ajaz, Abdel Nasser Tawfik, Zafar Wazir, Abd Al Karim Haj Ismail, Shi Jun Luo and Hafsa Zar Khan

Special Issue

Collectivity in High-Energy Proton-Proton and Heavy-Ion Collisions

Edited by

Prof. Dr. Khusniddin Olimov, Prof. Dr. Fu-Hu Liu and Prof. Dr. Kosim Olimov

MDPI

https://doi.org/10.3390/universe9010044

universe

MDPI

Article

Dependence of Freeze-Out Parameters on Collision Energies and Cross-Sections

Muhammad Waqas [1,*], Atef AbdelKader [2,3], Muhammad Ajaz [4], Abdel Nasser Tawfik [5], Zafar Wazir [6], Abd Al Karim Haj Ismail [2,3,*], Shi Jun Luo [1,7] and Hafsa Zar Khan [8]

1 School of Mathematics, Physics and Optoelectronic Engineering, Hubei University of Automotive Technology, Shiyan 442002, China
2 College of Humanities and Sciences, Ajman University, Ajman P.O. Box 346, United Arab Emirates
3 Nonlinear Dynamics Research Center (NDRC), Ajman University, Ajman P.O. Box 346, United Arab Emirates
4 Department of Physics, Abdul Wali Khan University Mardan, Mardan 23200, Pakistan
5 Faculty of Engineering, Future University in Egypt (FUE), Fifth Settlement, New Cairo 11835, Egypt
6 Department of Physics, Ghazi University, Dera Ghazi Khan 32200, Pakistan
7 Collaborative Center for Optoelectronic Technology, Hubei University of Automotive Technology, Shiyan 442002, China
8 Center for High Energy Physics, Punjab University, Lahore P.O. Box 54590, Pakistan
* Correspondence: waqas_phy313@yahoo.com or 20220073@huat.edu.cn (M.W.); a.hajismail@ajman.ac.ae (A.A.K.H.I.)

Abstract: We analyzed the transverse momentum spectra (p_T) reported by the NA61/SHINE and NA49 experiments in inelastic proton–proton (pp) and central Lead–Lead ($Pb-Pb$), Argon–Scandium ($Ar-Sc$), and Beryllium–Beryllium ($Be-Be$) collisions with the Blast-wave model with Boltzmann–Gibbs (BWBG) statistics. The BGBW model was in good agreement with the experimental data. We were able to extract the transverse flow velocity (β_T), the kinetic freeze-out temperature (T_0), and the kinetic freeze-out volume (V) from the p_T spectra using the BGBW model. Furthermore, we also obtained the initial temperature (T_i) and the mean transverse momentum ($<p_T>$) by the alternative method. We observed that T_0 increases with increasing collision energy and collision cross-section, representing the colliding system's size. The transverse flow velocity was observed to remain invariant with increasing collision energy, while it showed a random change with different collision cross-sections. In the same way, the kinetic freeze-out volume and mean transverse momentum increased with an increase in collision energy or collision cross-section. The same behavior was also seen in the freeze-out temperature, which increased with increasing collision cross-sections. At chemical freeze-out, we also determined both the chemical potential and temperature and compared these with the hadron resonance gas model (HRG) and different experimental data. We report that there is an excellent agreement with the HRG model and various experiments, which reveals the ability of the fit function to manifest features of the chemical freeze-out.

Keywords: transverse momentum spectra; kinetic freeze-out temperature; transverse flow velocity; kinetic freeze-out volume; initial temperature; collision cross-section

Citation: Waqas, M.; AbdelKader, A.; Ajaz, M.; Tawfik, A.N.; Wazir, Z.; Haj Ismail, A.A.K.; Luo, S.J.; Khan, H.Z. Dependence of Freeze-Out Parameters on Collision Energies and Cross-Sections. *Universe* **2023**, *9*, 44. https://doi.org/10.3390/universe9010044

Academic Editor: Antonino Del Popolo

Received: 17 November 2022
Revised: 5 January 2023
Accepted: 7 January 2023
Published: 10 January 2023

1. Introduction

In the early stages of nuclear collisions, a new state of matter, quark–gluon plasma (QGP), is likely to be formed under the extreme conditions of temperatures and densities. This matter has a lifetime of 7–10 fm/c, after which it changes quickly to a system of hadron gas. Due to multi-partonic interactions in the collision cross-section, information about the initial condition of the system is lost, such as the transverse excitation degree and the dynamic expansion of the collision cross-section. We can determine the final state behavior of such systems based on the number of particles produced and their energy and transverse momentum spectra.

During the evolution of heavy-ion collisions, the constituents of hot and dense matter interact with each other elastically or in-elastically and evolve into a new state of matter. This phenomenon of particle decoupling is called freeze-out, of which there are two kinds. Due to the expansion of the system, the inelastic collisions stop and the mean free path for the interactions becomes comparable to the size of the system. In addition, the abundances of different particle species become fixed. This is referred to as chemical freeze-out [1–3]. The chemical freeze-out stage is followed by the second kind. Although the relative fractions of the particles are fixed, at the chemical freeze-out stage, they continue to interact with each other until the final-state interactions between the particles are no longer effective. This is called the kinetic freeze-out where all interactions stop, and the transverse momentum spectra of the produced particles do not change. Therefore, the transverse momentum spectra of the particles are very important because they contain the necessary information about the final-state particles, including T_0, (β_T), (V), and the time of travel of the particles. At the chemical freeze-out stage, the chemical freeze-out temperature (T_{ch}) and baryon chemical potential (μ_b) can be determined based on well-defined thermodynamic conditions [3,4]. Besides T_0 and T_{ch}, T_i is also an important quantity because it determines the evolution of the entire colliding system.

Not only the systems with large collision cross-sections are conjectured to form QGP, small systems (especially with high multiplicity) are also expected to have such an effect. This is due to their small volumes of violent collision regions. At the top RHIC and LHC energies, pp collisions with high multiplicity show similar behavior to peripheral AA collisions, while at lower energies, from a few GeV to 10 GeV, the situation is different due to the dominance of baryons [5].

In the present work, we use the Blast-wave model with Boltzmann–Gibbs statistics [3,6–8] to analyze the transverse momentum spectra of the pions in various systems with different collision cross-sections at different energies and extract the kinetic freeze-out temperature, transverse flow velocity, and kinetic freeze-out volume. We will show the dependence of the above parameters on collision energy and collision cross-section. In the recent literature [3,7,9–23], the dependence of these parameters are in contradiction to one another. The contradiction involves the dependence of T_0 on the collision cross-section, which could increase, decrease, or be invariant from the central to the peripheral collisions (with increasing energy, especially for RHIC beam energies after 39 GeV). It is also worth mentioning that different models have been used by different groups and that the models are used under different conditions and constraints, leading to different results, as in [12]. In addition, there is a contradiction about the decoupling of the particles, which follow the single, double, triple, or multiple freeze-out scenarios, as in some cases, the particles' decoupling is reported to be affected by the coalescence and iso-spin symmetry. In fact, it is always very useful to conduct more studies on these topics and try to finalize some corroborative conclusions. Moreover, we will also extract T_i, T_{ch}, and T_0. Furthermore, the $\langle p_T \rangle$ shall be extracted. This allows us to study their dependence on collision energy and cross-section.

Before going to the next section, we would like to point out that we chose the Blast-wave model with Boltzmann–Gibbs statistics in the present work because it is the most direct and simpler model with fewer parameters, as well as being closer to the ideal gas model [24–28]. In addition, the performance of the BGBW model is good in the low p_T region (p_T = 0–3.4 or 4 GeV/c) and meets the needs of this research, and the reason behind the selection of pions is that the temperature obtained from their spectra is closest to the source temperature. The rest of this paper is organized as follows: The methods and models are discussed in Section 2. The results and discussions are presented in Section 3. The summary and conclusion are described in Section 4.

2. Methods and Models

In high-energy collisions, the p_T spectra of the produced particles are very complex since the function describing p_T can have different forms. The complex p_T structure refers

to different p_T regions, which correspond to different interaction mechanisms and have different properties. These regions include the $p_T <$ 4–6 GeV/c as the first region, followed by the second region in the energy range from $p_T >$ 4–6 GeV/c to $p_T <$ 20 GeV/c, and the third region is $p_T >$ 20 GeV/c. The effects and changes by the medium appear in the first p_T region, while they are weak in the second p_T range, while the third p_T region shows the negligible influence of the medium given by the nuclear transparency. In addition, it is not enough to use a single probability density function to describe the p_T spectra [29]. There are various p_T regions [30] according to the model analysis that is described in our previous work [31]. Soft excitation and hard scattering are the two main processes for particle production. The soft excitation process results in the production of most light flavor particles, whose p_T range is narrow (less than 2–3 GeV/c), while the hard scattering process exists in a wide p_T range ($p_T >$ 3 GeV/c); in addition, some light flavor particles are also produced in this process. In some cases of not-too-high collision energies, the hard scattering process can be underestimated, and soft excitation plays the main role in particle production. In general, due to the small fraction of the hard process in the narrow p_T range, the hard scattering process does not contribute to temperature or flow velocity. For the soft excitation process, we have various choices of formalism, which include, but are not limited to, the standard distribution [32], Tsallis statistics [33–36], Erlang distribution [37–39], the Schwinger mechanism [40–43], the Blast-wave model with Boltzmann–Gibbs statistics [6,44], the Blast-wave model with Tsallis statistics [45–47], and Hagedorn thermal model distribution [48].

In the present work, we use the Blast-wave model with Boltzmann–Gibbs statistics, which assumes that the particles are locally thermalized at the thermal/kinetic freeze-out temperature and that they are moving with common transverse collective flow velocities [5,49]. Let us assume a thermal source, which is radially boosted, has T_0 and β_T, and the p_T spectra distribution of the particles is given as:

$$\begin{aligned} f(p_T) &= \frac{1}{N}\frac{dN}{dp_T} = \frac{1}{N}\frac{gV}{(2\pi)^2} p_T m_T \int_0^R r dr \\ &\times I_0\left[\frac{p_T \sinh(\rho)}{T_0}\right] K_1\left[\frac{m_T \cosh(\rho)}{T_0}\right], \end{aligned} \quad (1)$$

where m_T ($m_T = \sqrt{p_T^2 + m_0^2}$) represents the transverse mass of the particles, and g is the spin degeneracy factor of the particle ($g = 1$ for pions, for example). I_0 and K_1 are the modified Bessel function of the first and second kind, respectively. The radial flow velocity profile, ρ, is defined as $\tanh^{-1}[\beta(r)]$, where r/R represents the relative radial position in thermal source. The average $\beta(r)$ can be obtained from $\langle\beta_T\rangle$=2$\beta_S/(n_0+2)$, where n_0 is the self similar flow velocity profile, and its value can be 1 [5] or 2 [50], or it may also be considered as a free parameter [49]. In some cases, it is possible that BGBW does not fit the whole p_T region, then we use the two-component model [17,31].

In the fit process, the extracted parameters usually have a correlation, such as T_0, which becomes larger in some cases, and a smaller β_T can lead to similar results if a smaller T_0 and larger β_T are used. This is due to the influence of the p_T range and also n_0 if taken as a free parameter. To reduce the effect of such a correlation, we need to analyze the $\langle p_T\rangle$ and the root-mean-square p_T over $\sqrt{2}(\sqrt{\langle p_T^2\rangle/2})$. We can calculate $\langle p_T\rangle$ and $\sqrt{\langle p_T^2\rangle/2}$ from the fit function over a given p_T range, where $\sqrt{\langle p_T^2\rangle/2}$ is the initial temperature of the interacting system according to the string percolation model [51–53].

3. Results and Discussion

The transverse momentum (p_T) spectra of π^- mesons produced in inelastic (INEL) proton–proton (pp), Beryllium–Beryllium (Be–Be), Argon–Scandium (Ar–Sc), and Lead–Lead (Pb–Pb) collisions, at different energies, are presented in Figure 1 (top panels (a) and (b) show the p_T spectra of the pions in inelastic (INEL) pp collisions and the most central Be–

Be, Ar–Sc, and Pb–Pb collisions, respectively, at $|y| = 0.1$ rapidity). The symbols represent the experimental data of the NA61/SHINE [54–56] and NA49 experiments [57,58] measured at SPS CERN. The curve represents the results of our fit by the Blast-wave model with Boltzmann–Gibbs statistics. One can see that Equation (1) can describe the experimental data well, and the related parameters are extracted from the fit of Equation (1) to the experimental data following the least-squares method. We checked the stability of the obtained parameter values by repeating the fit procedures three times and changing the initial values of the parameters. As a result, the stability of the obtained parameters was fully confirmed (they stayed practically the same). The data in Figure 1 (panel (a), (b), and (c)) are taken from ref. [54–56], respectively, while the data in Figure 1 (panel (d)) are taken from ref. [57,58]. To see the fit results clearly, the spectra of the pions in pp collisions at 40, 80, and 158 A GeV/c in panel (a) are scaled by 4, 14, and 40, respectively. In panel (b), at 30, 40, and 150 A GeV/c, the spectra are scaled by 4, 2, and 1/8, respectively. In panel (c), at 40, 80, and 160 A GeV/c, the spectra are scaled by 20, 8, and 4, respectively. Furthermore, we would like to mention that in Figure 1, we are using the hydrodynamical model to fit the experimental spectra, which is not available at these energies, which results in few data points at high energies. However, if there are more data points in the same pt range, it will improve the quality of the fit but will not have a large effect on the final results. Moreover, if the p_T range is to be changed, this might have an effect on the results.

The lower layer in each panel represents the corresponding ratio of data/fit. The related values of free parameters and χ^2 and the degrees of freedom (dof) are presented in Table 1. One can see that Equation (1) provides an approximate well fit to the data in all collisions at all energies. In Table 1, it should be noted that different rapidity could be used from [54] for pp collisions, where the data points are comparatively more, but we only used the rapidity $|y| = 0.1$ in the present work because the data for pp, Be–Be, Ar–Sc, and Pb–Pb collisions for another similar rapidity are not available. The change in rapidity will have an effect on the collective parameters [59], while the present work is focused on the dependence of the collective parameters on collision energies and collisions cross-sections. In addition, N_0, used in the table, is a normalization constant that compares the fit function with the experimental spectra.

In the present work, the data/fit ratio is in the acceptable range. In some cases, especially in the lower panels of Figure 1, the data/fit ratio is slightly larger than 2. The larger tension of the data to the curve from unity is in the very low p_T range of $p_T < 0.5$ GeV/c. The reason for this is that $pT < 0.5$ GeV/c is the very soft region where a large fraction of pions originate from resonance decay, which is not covered by the model. It is true that if the data/fit ratio is close to unity, this will give us the confidence that the model used can describe the data very well, but this is mostly possible in the case that we use the two components of the model. However, the contribution of the second component of the model to the parameters is very little; therefore, we do not consider using it in the present work. To study the change in the trend of the parameters, Figure 2 shows the dependencies of the kinetic freeze-out temperature, transverse flow velocity, and kinetic freeze-out volume on collision energy and collision cross-section. The panels (a), (b), and (c) show the result of the T_0, β_T, and V, respectively. The different symbols represent different systems. The trend of the parameters from left to right shows the energy dependence of the corresponding parameter, while from up to down, their dependence on collision cross-section is displayed. In panel (a), the dependence of the kinetic freeze-out temperature on the collision energy and collision cross-section is shown. We can observe that as the collision energy increases, T_0 also increases. The reason behind this is that at high energies, the collision is very violent, which gives a higher excitation to the system. The higher the energies, the higher the degree of excitation the system will obtain. Furthermore, it can also be observed that T_0 in pp collisions is less than in the other three collisions, while in Pb–Pb, it is the largest, followed by Ar–Sc and then Be–Be collisions. This indicates that T_0 depends on the collision cross-section interaction. The larger the collision cross-section, the higher the T_0 we observe. The proton–proton system has a smaller cross-section, while

the Lead–Lead system has the largest collision cross-section and, thus, the largest T_0 value. This is in agreement with the results in [13]. Panel (b) shows the dependence of β_T on the energy and collision cross-section. At present, we observe that β_T remains unchanged with increasing collision energy. We believe that this is due to the reason that collective behavior does not change with increasing energy. In addition, β_T changes randomly for every system, as reported in the literature [60,61]. In the present case, no dependence of β_T can be observed on the collision cross-section. β_T is normally taught to be a decreasing function with increasing cross-section because denser systems should have lower flow, but at the same time, higher pressure in the system tends to increase it. Therefore, there is no dependence of β_T observed on the collision cross-section. In panel (c), the dependence of V on the collision energy and the collision cross-section is presented. One can see that V increases as the collision energy increases. The reason behind this is that there is a larger initial bulk system at high energies. The increase in energy results in a long evolution time, which corresponds to a larger partonic system, and V becomes larger in a large partonic system. Furthermore, we can also observe that V is larger for Pb–Pb collisions, followed by Ar–Sc and then Be–Be collisions, and it is the lowest in pp collisions. This indicates its dependence on the collision cross-section (the size of the interacting system).

Table 1. List of the parameters. The "-" sign is used in some places instead of dof. In fact, it is not the fit result. If dof < 0, we use "-" instead of negative values.)

Collisions	Energy	T_0 (GeV)	β_T (c)	V (fm^3)	N_0	χ^2/dof
Figure 1a	20 GeV	0.085 ± 0.004	0.300 ± 0.010	1000 ± 110	0.27 ± 0.04	2/3
pp	31 GeV	0.092 ± 0.005	0.302 ± 0.009	1200 ± 110	1.4 ± 0.3	0.2/-
	40 GeV	0.097 ± 0.005	0.308 ± 0.008	1340 ± 102	1.9 ± 0.3	1/-
	80 GeV	0.103 ± 0.006	0.304 ± 0.008	1513 ± 100	2 ± 0.4	0.03/-
	158 GeV	0.108 ± 0.005	0.308 ± 0.011	1600 ± 95	2 ± 0.4	0.1/1
Figure 1b	19 GeV	0.100 ± 0.006	0.335 ± 0.007	1400 ± 100	0.0062 ± 0.0004	1/13
Be–Be	31 GeV	0.107 ± 0.006	0.334 ± 0.008	1500 ± 120	0.0063 ± 0.0003	5/14
	40 GeV	0.114 ± 0.005	0.335 ± 0.008	1645 ± 110	0.000075 ± 0.000004	3/14
	75 GeV	0.120 ± 0.006	0.336 ± 0.009	1900 ± 108	$8.5{\times}10^{-6} \pm 5 \times 10^{-7}$	4/14
	150 GeV	0.125 ± 0.006	0.340 ± 0.007	2100 ± 150	$8.9 \times 10^{-6} \pm 4 \times 10^{-7}$	1.5/14
Figure 1c	13 GeV	0.104 ± 0.004	0.250 ± 0.010	2100 ± 127	$1.5 \times 10^{-4} \pm 4 \times 10^{-5}$	13/16
Ar–Sc	19 GeV	0.115 ± 0.005	0.240 ± 0.009	2200 ± 130	0.00154 ± 0.0004	11/16
	30 GeV	0.123 ± 0.006	0.252 ± 0.008	2320 ± 120	0.019 ± 0.004	8/16
	40 GeV	0.130 ± 0.005	0.240 ± 0.008	2500 ± 119	0.18 ± 0.03	12/16
	75 GeV	0.136 ± 0.005	0.240 ± 0.009	2700 ± 120	2 ± 0.3	37/16
	150 GeV	0.141 ± 0.004	0.180 ± 0.008	2900 ± 130	20 ± 4	12/16
Figure 1d	20 GeV	0.133 ± 0.005	0.140 ± 0.007	2900 ± 140	55 ± 8	45/12
Pb–Pb	30 GeV	0.139 ± 0.005	0.145 ± 0.007	3100 ± 152	300 ± 32	36/12
	40 GeV	0.145 ± 0.005	0.128 ± 0.007	3274 ± 147	58 ± 9	23/10
	80 GeV	0.157 ± 0.004	0.130 ± 0.008	3400 ± 138	770 ± 100	12/10
	160 GeV	0.163 ± 0.006	0.130 ± 0.008	3700 ± 143	9000 ± 800	15/10

Figure 3a shows the dependence of $\langle p_T \rangle$ and T_i on collision energy and collision cross-section. One can see that $\langle p_T \rangle$ increases with increasing collision energy and also in the collision cross-section because larger momentum (energy) is transferred at higher energies and large collision cross-sections, which results in further multiple scattering. However, in Figure 3b, the dependence of T_i on energy and collision cross-section is presented. One can see that T_i increases with increasing collision energy and is larger for a large collision cross-section system.

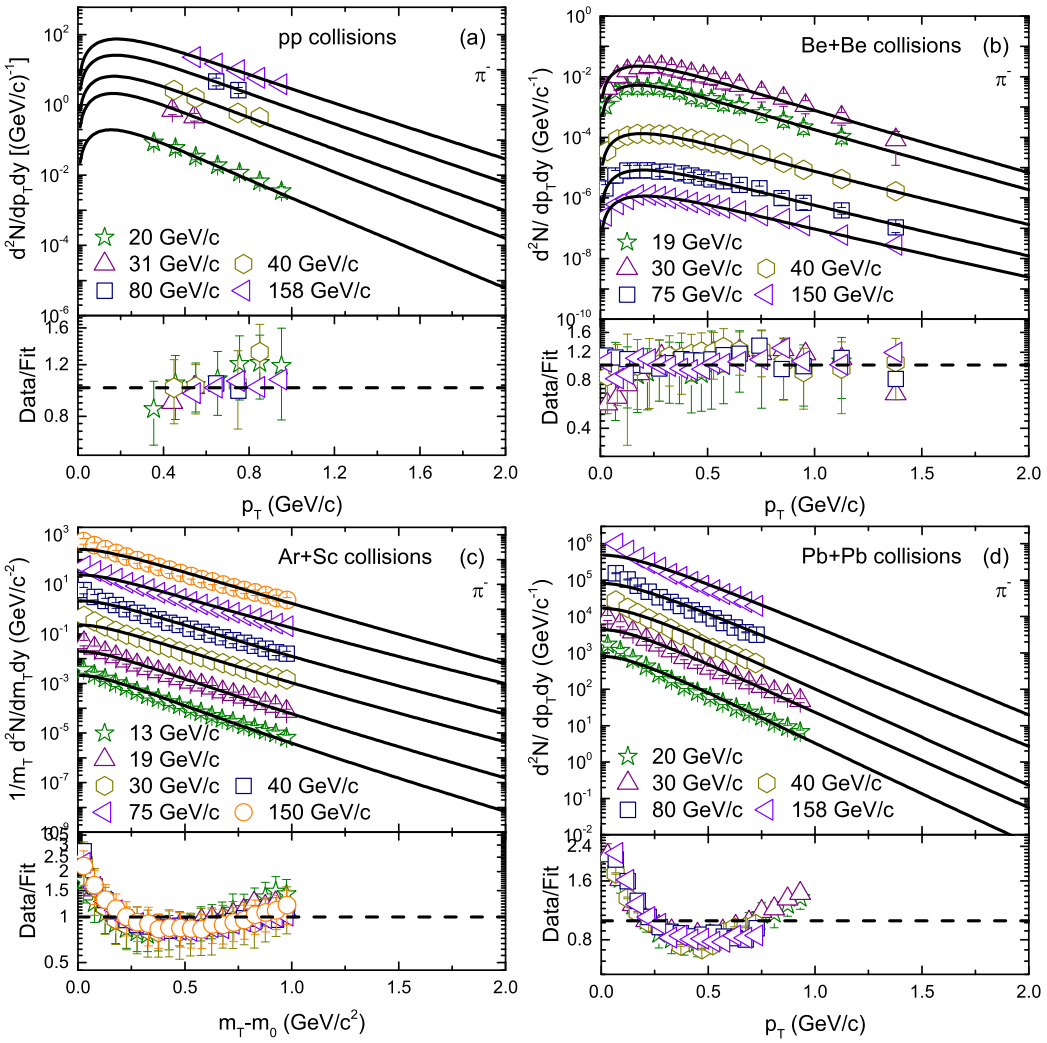

Figure 1. Transverse momentum spectra of π^- produced in pp, and the most central Be−Be, Ar−Sc, and Pb−Pb collisions at different energies at $|y| = 0.1$ rapidity interval. The symbols are the experimental data of the NA61/SHINE [54–56] and NA49 experiments [54–56,58] measured by SPS CERN. The curves represent our fit by Equation (1). The corresponding data/fit ratios are followed in each panel.

We observe that T_i is larger than T_0. Generally, T_i is larger than the effective temperature (T_{eff}), and T_{eff}, in turn, is larger than T_0 because T_{eff} includes the flow effect.

The other kind of freeze-out parameters—the temperature and baryon chemical potential, at chemical freeze-out—could be parameterized by various thermodynamics conditions, such as constant entropy density normalized to temperature cubed, constant higher-order moments of particle multiplicities, and constant trace anomaly (interaction rate) [62–64]. The present study suggests that

$$T_{ch} = \frac{T_{\rm lim}}{1+\exp[2.60-\ln(\sqrt{s_{NN}})/0.45]}, \quad (2)$$

$$\mu_b = \frac{1.303}{1+0.286\sqrt{s_{NN}}}, \quad (3)$$

where $T_{\rm lim} = 0.158$ GeV and $\sqrt{s_{NN}}$ are in the units of GeV [65]. The chemical freeze-out temperature is conjectured to lay between T_i and T_0, generally. It is slightly larger than or approximately equal to T_{eff}. Such an order is in agreement with the order of time evolution of the interacting system. Figure 4 depicts T_{ch} vs. μ_b and compares these results with the

experimental data and the hadron resonance gas model (HRG) [24]. With the experimental results, we mean T_{ch} and μ_b in thermal models, such as the HRG model, fulfilling certain thermodynamic conditions and best reproducing the measurement of many particle ratios at various energies. Focusing on particle ratios largely eliminates the volume of the statistical system. The curve label "This work" is the result determined by the statistical hadronization model fits. The thin curve represents the results obtained by the HRG model under the condition of constant higher-order moments of particle multiplicities [62,63,66]. It should be mentioned that in creating this graph, we have included calculations across a very wide range of energies, exceeding the NA61/SHINE and NA49 energies. The latter is limited to a short range of T_{ch} and μ_b. The excellent agreement with both the HRG model and various experiments reveals the ability of the Blast-wave model with Boltzmann–Gibbs statistics to manifest the features of the chemical freeze-out.

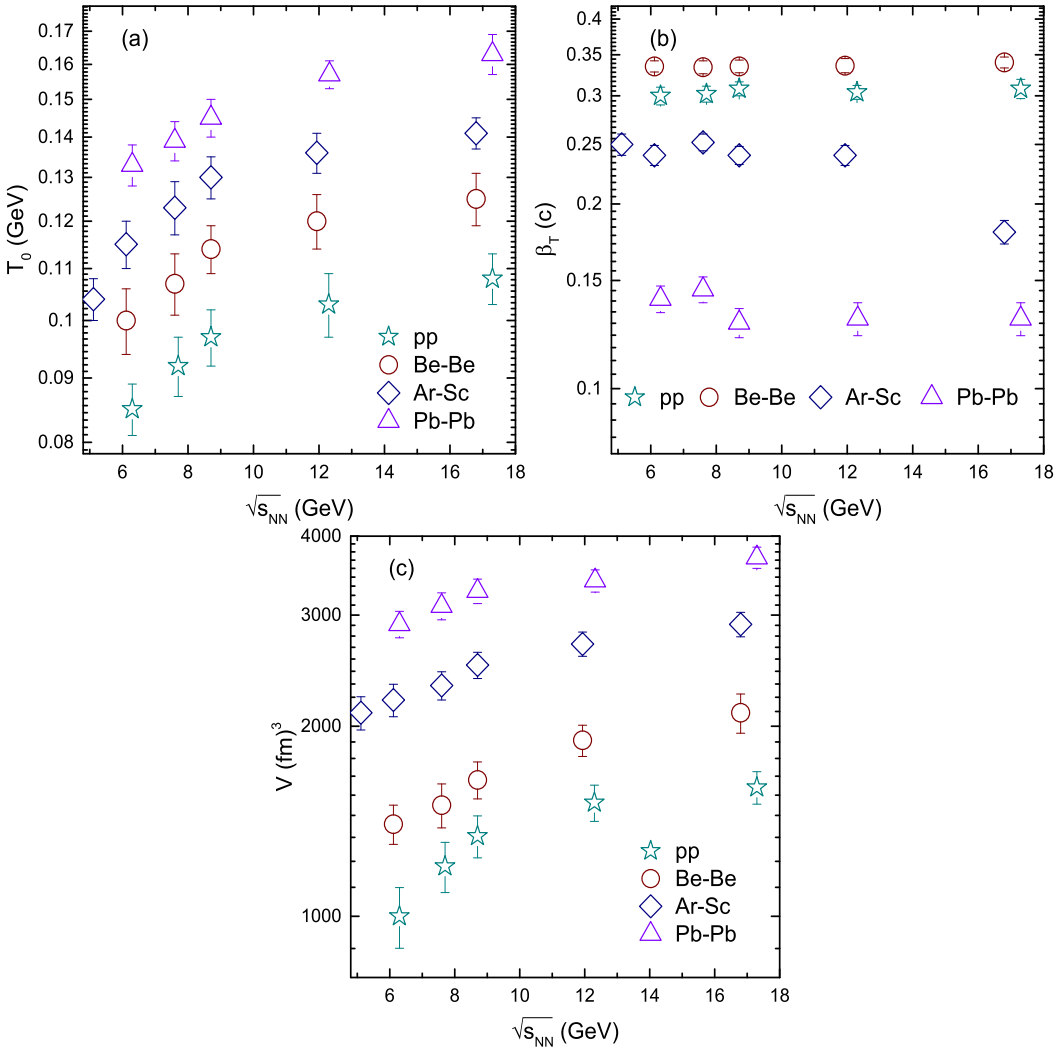

Figure 2. Dependence of (**a**) kinetic freeze-out temperature, (**b**) transverse flow velocity, and (**c**) kinetic freeze-out volume on collision energy and collision cross-section.

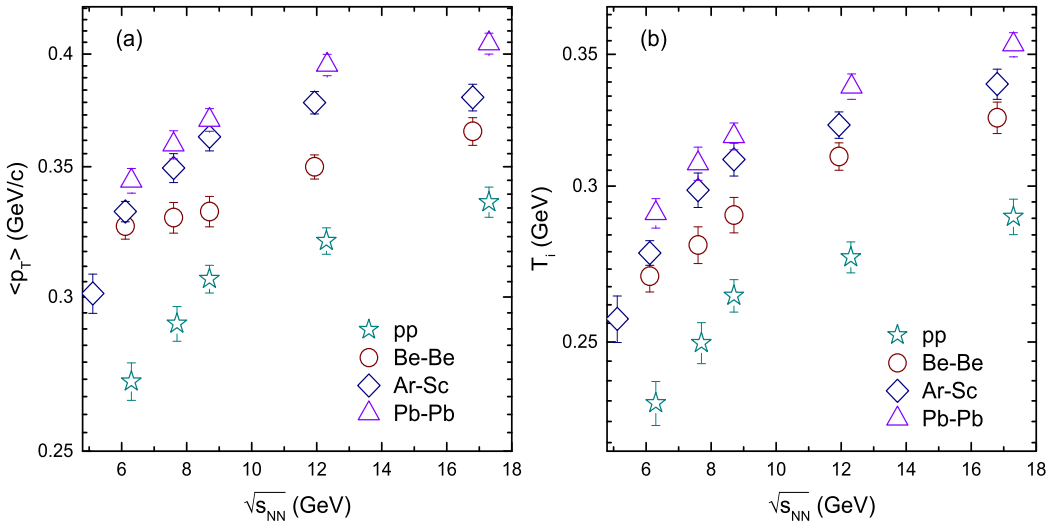

Figure 3. Dependence of (**a**) mean transverse momentum and (**b**) initial temperature on collision energy and collision cross-section.

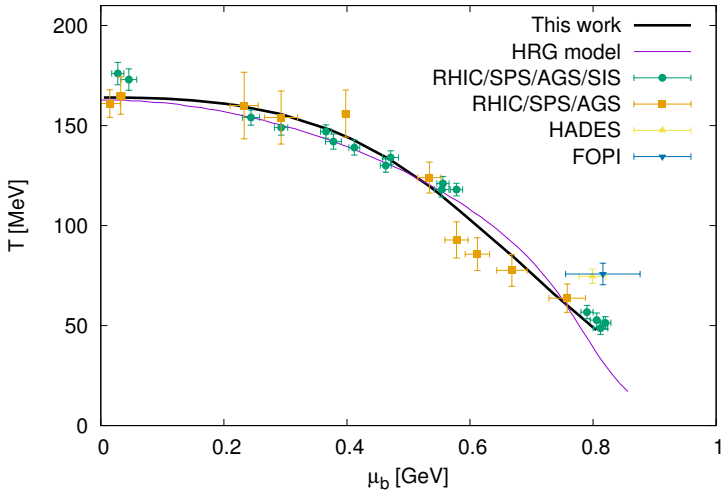

Figure 4. Dependence of the chemical freeze-out temperature on the baryon chemical potential, Equation (1) and Equation (2), respectively. The symbols represent various measurements. The thin curve stands for results obtained by the HRG model at constant higher-order moments of particle multiplicities. The curve label "This work" in the legend is determined by the statistical hadronization model fits.

4. Summary and Conclusions

We summarize here our main observations and conclusions as follows:

- The transverse momentum spectra of pions produced in inelastic proton–proton and most central Be–Be, Ar–Sc, and Pb–Pb collisions at different energies were studied by the Blast-wave model with Boltzmann–Gibbs statistics. The results are in agreement with the experimental data measured by the NA61/SHINE and NA49 experiments at SPS energies. In addition, we extracted the kinetic freeze-out temperature T_0, the initial temperature T_i, the transverse flow velocity β_T, and the kinetic freeze-out volume V.
- We studied the dependence of T_0 and T_i on collision energy and cross-section. T_0 and T_i were found to increase with the increase in collision energy and collision cross-section. This increase is due to the transfer of more energy in the system at higher energies and in large colliding systems.

- β_T was observed to remain constant with the increase in energy due to the invariant collective flow with increasing energy. There is no dependence of transverse flow velocity on the collision cross-section.
- V was found to increase with increasing collision energy because of the large initial bulk at higher energies, and it was also larger for large collision cross-sections. Furthermore, the mean transverse momentum increased with increasing collision energy due to a greater transfer of energy in the system at higher energies. It was also observed that mean transverse momentum was larger for the systems with large collision cross-sections because, in large collision section systems, the transfer of energy is larger.
- Finally, the chemical potential and temperature show excellent agreement in comparison to the HRG model and different experimental data at the chemical freeze-out, revealing the ability of the Blast-wave model with Boltzmann–Gibbs statistics to manifest features of the chemical freeze-out.

Author Contributions: Conceptualization, M.W., A.A.K.H.I. and M.A.; methodology, M.W., A.A.K.H.I. and A.A.; software, M.A., A.A.K.H.I. and A.A.; validation, M.A., M.W., A.N.T., S.J.L. and A.A.K.H.I.; formal analysis, A.N.T., S.J.L., H.Z.K. and Z.W.; investigation, A.A.K.H.I., Z.W., H.Z.K. and A.A.; resources, M.A. and A.A.; writing—original draft preparation, M.W., A.A.K.H.I. and M.W. All authors have read and agreed to the final published version of the manuscript.

Funding: This research was funded by Ajman University, Deanship of Research and Graduate Studies, Internal Research Grant No: (DGSR Ref. 2022-IRG-HBS-11).

Institutional Review Board Statement: Not applicable.

Informed Consent Statement: Not applicable.

Data Availability Statement: Not applicable.

Acknowledgments: This work was supported by Ajman University Internal Research Grant No. (DGSR Ref. 2022-IRG-HBS-11).

Conflicts of Interest: The authors declare no conflict of interest.

References

1. Liu, F.H.; Fakhraddin, S.; Lacey, R.A.; Sahoo, R.; Sarkisyan-Grinbaum, E.K.; Singh, B.K. Properties of Chemical and Kinetic Freeze-Outs in High-Energy Nuclear Collisions. *Adv. High Energy Phys.* **2018**, *2018*, 9184574. [CrossRef]
2. Xu, J.; Ko, C.M. Chemical freeze-out in relativistic heavy-ion collisions. *Phys. Lett. B* **2017**, *772*, 290–293. . j.physletb.2017.06.061. [CrossRef]
3. Tawfik, A.N.; Yassin, H.; Elyazeed, E.R.A. Chemical freeze-out in Hawking-Unruh radiation and quark-hadron transition. *Phys. Rev. D* **2015**, *92*, 085002,
4. Tawfik, A. The Influence of strange quarks on QCD phase diagram and chemical freeze-out: Results from the hadron resonance gas model. *J. Phys. G* **2005**, *31*, S1105–S1110.
5. Lao, H.L.; Liu, F.H.; Li, B.C.; Duan, M.Y.; Lacey, R.A. Examining the model dependence of the determination of kinetic freeze-out temperature and transverse flow velocity in small collision system. *Nucl. Sci. Tech.* **2018**, *29*, 164.
6. Schnedermann, E.; Sollfrank, J.; Heinz, U.W. Thermal phenomenology of hadrons from 200 to A/GeV S+S collisions. *Phys. Rev. C* **1993**, *48*, 2462–2475.
7. Zhang, S.; Ma, Y.G.; Chen, J.H.; Zhong, C. Production of Kaon and Λ in Nucleus-Nucleus Collisions at Ultrarelativistic Energy from a Blast-Wave Model. *Adv. High Energy Phys.* **2015**, *2015*, 460590.
8. Ajaz, M.; Khubrani, A.M.; Waqas, M.; Haj Ismail, A.A.K.; Dawi, E.A. Collective properties of hadrons in comparison of models prediction in pp collisions at 7 TeV. *Results Phys.* **2022**, *36*, 105433. [CrossRef]
9. Abelev, B.; Adam, J.; Adamová, D.; Adare, A.M.; Aggarwal, M.M.; Rinella, G.A.; Agocs, A.G.; Agostinelli, A.; Salazar, S.A.; Ahammed, Z.; et al. Pion, Kaon, and Proton Production in Central Pb–Pb Collisions at $\sqrt{s_{NN}} = 2.76$ TeV. *Phys. Rev. Lett.* **2012**, *109*, 252301.
10. Das, S. Centrality dependence of freeze-out parameters from the beam energy scan at STAR. *Nucl. Phys. A* **2013**, *904–905*, 891c–894c,
11. Das, S. Identified particle production and freeze-out properties in heavy-ion collisions at RHIC Beam Energy Scan program. *EPJ Web Conf.* **2015**, *90*, 08007.

12. Adamczyk, L.; Adkins, J.K.; Agakishiev, G.; Aggarwal, M.M.; Ahammed, Z.; Ajitanand, N.N.; Alekseev, I.; Anderson, D.M.; Aoyama, R.; Aparin, A.; et al. Bulk Properties of the Medium Produced in Relativistic Heavy-Ion Collisions from the Beam Energy Scan Program. *Phys. Rev. C* **2017**, *96*, 044904.
13. Zhang, S.; Ma, Y.G.; Chen, J.H.; Zhong, C. Beam energy dependence of Hanbury-Brown-Twiss radii from a blast-wave model. *Adv. High Energy Phys.* **2016**, *2016*, 9414239.
14. Chatterjee, S.; Das, S.; Kumar, L.; Mishra, D.; Mohanty, B.; Sahoo, R.; Sharma, N. Freeze-Out Parameters in Heavy-Ion Collisions at AGS, SPS, RHIC, and LHC Energies. *Adv. High Energy Phys.* **2015**, *2015*, 349013. [CrossRef]
15. Luo, X. Exploring the QCD Phase Structure with Beam Energy Scan in Heavy-ion Collisions. *Nucl. Phys. A* **2016**, *956*, 75–82.
16. Lao, H.L.; Liu, F.H.; Li, B.C.; Duan, M.Y. Kinetic freeze-out temperatures in central and peripheral collisions: Which one is larger? *Nucl. Sci. Tech.* **2018**, *29*, 82.
17. Waqas, M.; Peng, G.X.; Liu, F.H. An evidence of triple kinetic freezeout scenario observed in all centrality intervals in Cu–Cu, Au–Au and Pb–Pb collisions at high energies. *J. Phys. G* **2021**, *48*, 075108.
18. Waqas, M.; Peng, G.X.; Liu, F.H.; Wazir, Z. Effects of coalescence and isospin symmetry on the freezeout of light nuclei and their anti-particles. *Sci. Rep.* **2021**, *11*, 20252.
19. Haj Ismail, A. Monte Carlo simulation of the cosmic muon charge ratio. *Kuwait J. Sci.* **2022**, *49*, 1–8. . 49i1.11497. [CrossRef]
20. Alba, P.; Bellwied, R.; Mantovani-Sarti, V.; Noronha-Hostler, J.; Parotto, P.; Portillo-Vazquez, I.; Ratti, C.; Stafford, J.M. Chemical freeze-out parameters of net-kaons in heavy-ion collisions. *Nucl. Phys. A* **2021**, *1005*, 121865. . 2020.121865. [CrossRef]
21. Ajaz, M.; Waqas, M.; Peng, G.X.; Yasin, Z.; Younis, H.; Haj Ismail, A.A.K. Study of p_T spectra of light particles using modified Hagedorn function and cosmic rays Monte Carlo event generators in proton–proton collisions at $\sqrt{s}$ = 900 GeV. *Eur. Phys. J. Plus* **2022**, *137*, 52.
22. Li, L.L.; Haj Ismail, A.A.K. Study of Bulk Properties of Strange Particles in Au+Au Collisions at sNN = 54.4 GeV. *Entropy* **2022**, *24*, 1720. [CrossRef] [PubMed]
23. Bugaev, K.A.; Oliinychenko, D.R.; Cleymans, J.; Ivanytskyi, A.I.; Mishustin, I.N.; Nikonov, E.G.; Sagun, V.V. Chemical Freeze-out of Strange Particles and Possible Root of Strangeness Suppression. *EPL* **2013**, *104*, 22002.
24. Tawfik, A.N. Equilibrium statistical-thermal models in high-energy physics. *Int. J. Mod. Phys. A* **2014**, *29*, 1430021.
25. Tawfik, A.N. Koppe's Work of 1948: A fundamental for non-equilibrium rate of particle production. *Z. Naturforsch. A* **2014**, *69*, 106–107.
26. Karsch, F.; Redlich, K.; Tawfik, A. Thermodynamics at nonzero baryon number density: A Comparison of lattice and hadron resonance gas model calculations. *Phys. Lett. B* **2003**, *571*, 67–74.
27. Karsch, F.; Redlich, K.; Tawfik, A. Hadron resonance mass spectrum and lattice QCD thermodynamics. *Eur. Phys. J. C* **2003**, *29*, 549–556.
28. Adamovich, M.I.; Aggarwal, M.M.; Alexandrov, Y.A.; Amirikas, R.; Andreeva, N.P.; Anzon, Z.V.; Arora, R.; Avetyan, F.A.; Badyal, S.K.; Bakich, A.M.; et al. Produced particle multiplicity dependence on centrality in nucleus-nucleus collisions. *J. Phys. G* **1996**, *22*, 1469–1481. [CrossRef]
29. Chatrchyan, S.; The CMS Collaboration; Khachatryan, V.; Sirunyan, A.M.; Tumasyan, A.; Adam, W.; Aguilo, E.; Bergauer, T.; Dragicevic, M.; Erö, J.; et al. Measurement of the Relative Prompt Production Rate of χ_{c2} and χ_{c1} in pp Collisions at $\sqrt{s} = 7$ TeV. *Eur. Phys. J. C* **2012**, *72*, 2251.
30. Suleymanov, M. The meaning behind observed p_T regions at the LHC energies. *Int. J. Mod. Phys. E* **2018**, *27*, 1850008.
31. Waqas, M.; Peng, G.X. Study of Proton, Deuteron, and Triton at 54.4 GeV. *Adv. High Energy Phys.* **2021**, *2021*, 6674470.
32. Cleymans, J.; Worku, D. Relativistic Thermodynamics: Transverse Momentum Distributions in High-Energy Physics. *Eur. Phys. J. A* **2012**, *48*, 160.
33. Tsallis, C. Possible Generalization of Boltzmann-Gibbs Statistics. *J. Statist. Phys.* **1988**, *52*, 479–487. . 16429. [CrossRef]
34. Biro, T.S.; Purcsel, G.; Urmossy, K. Non-Extensive Approach to Quark Matter. *Eur. Phys. J. A* **2009**, *40*, 325–340.
35. Zheng, H.; Zhu, L. Comparing the Tsallis Distribution with and without Thermodynamical Description in $p + p$ Collisions. *Adv. High Energy Phys.* **2016**, *2016*, 9632126,
36. Ajaz, M.; Ismail, A.A.K.H.; Ahmed, A.; Wazir, Z.; Shehzadi, R.; Younis, H.; Khan, G.; Khan, R.; Ali, S.; Waqas, M.; et al. Centrality dependence of PT distributions and nuclear modification factor of charged particles in Pb–Pb interactions at SNN = 2.76 TeV. *Results Phys.* **2021**, *30*, 104790. [CrossRef]
37. Liu, F.H.; Gao, Y.Q.; Tian, T.; Li, B.C. Unified description of transverse momentum spectrums contributed by soft and hard processes in high-energy nuclear collisions. *Eur. Phys. J. A* **2014**, *50*, 94. [CrossRef]
38. Gao, L.N.; Liu, F.H.; Lacey, R.A. Excitation functions of parameters in Erlang distribution, Schwinger mechanism, and Tsallis statistics in RHIC BES program. *Eur. Phys. J. A* **2016**, *52*, 137.
39. Xie, W.J. Transverse momentum spectra in high-energy nucleus-nucleus, proton-nucleus and proton-proton collisions. *Chin. Phys. C* **2011**, *35*, 1111–1119. [CrossRef]
40. Schwinger, J.S. On gauge invariance and vacuum polarization. *Phys. Rev.* **1951**, *82*, 664–679. . 664. [CrossRef]
41. Wang, R.C.; Wong, C.Y. Finite Size Effect in the Schwinger Particle Production Mechanism. *Phys. Rev. D* **1988**, *38*, 348–359. [CrossRef] [PubMed]
42. Wong, C.Y. *Introduction to High-Energy Heavy Ion Collisions*; World Scientific Publishing Co.: Singapore, 1995.

43. Braun-Munzinger, P.; Redlich, K.; Stachel, J. Particle production in heavy ion collisions. In *Quark-Gluon Plasma 3*; World Scientific Publishing Co.: Singapore, 2003; pp. 491–599. ._0008. [CrossRef]
44. Abelev, B.I.; Aggarwal, M.M.; Ahammed, Z.; Alakhverdyants, A.V.; Anderson, B.D.; Arkhipkin, D.; Averichev, G.S.; Balewski, J.; Barannikova, O.; Barnby, L.S.; et al. Identified particle production, azimuthal anisotropy, and interferometry measurements in Au+Au collisions at s(NN)**(1/2) = 9.2- GeV. *Phys. Rev. C* **2010**, *81*, 024911.
45. Tang, Z.; Xu, Y.; Ruan, L.; van Buren, G.; Wang, F.; Xu, Z. Spectra and radial flow at RHIC with Tsallis statistics in a Blast-Wave description. *Phys. Rev. C* **2009**, *79*, 051901.
46. Tang, Z.; Yi, L.; Ruan, L.; Shao, M.; Chen, H.; Li, C.; Mohanty, B.; Sorensen, P.; Tang, A.; Xu, Z. Statistical Origin of Constituent-Quark Scaling in the QGP hadronization. *Chin. Phys. Lett.* **2013**, *30*, 031201.
47. Jiang, K.; Zhu, Y.; Liu, W.; Chen, H.; Li, C.; Ruan, L.; Tang, Z.; Xu, Z.; Xu, Z. Onset of radial flow in p+p collisions. *Phys. Rev. C* **2015**, *91*, 024910.
48. Dogra, S.M. Particle Production and Correlations in Ultra-Relativistic Nucleus-Nucleus Collisions. Ph.D. Thesis, Jammu University, Jammu, India, 2008.
49. Petrovici, M.; Andrei, C.; Berceanu, I.; Bercuci, A.; Herghelegiu, A.; Pop, A. Recent results and open questions on collective type phenomena from A-A to pp collisions. *AIP Conf. Proc.* **2015**, *1645*, 52–60.
50. Adam, J.; Adamczyk, L.; Adams, J.R.; Adkins, J.K.; Agakishiev, G.; Aggarwal, M.M.; Ahammed, Z.; Alekseev, I.; Anderson, D.M.; Aoyama, R.; et al. Strange hadron production in Au+Au collisions at $\sqrt{s_{NN}}$ = 7.7, 11.5, 19.6, 27, and 39 GeV. *Phys. Rev. C* **2020**, *102*, 034909.
51. Gutay, L.J.; Hirsch, A.S.; Pajares, C.; Scharenberg, R.P.; Srivastava, B.K. De-Confinement in small systems: Clustering of color sources in high multiplicity $\bar{p}$p collisions at $\sqrt{s}$= 1.8 TeV. *Int. J. Mod. Phys. E* **2015**, *24*, 1550101.
52. Scharenberg, R.P.; Srivastava, B.K.; Pajares, C. Exploring the initial stage of high multiplicity proton-proton collisions by determining the initial temperature of the quark-gluon plasma. *Phys. Rev. D* **2019**, *100*, 114040. . 040. [CrossRef]
53. Sahoo, P.; De, S.; Tiwari, S.K.; Sahoo, R. Energy and Centrality Dependent Study of Deconfinement Phase Transition in a Color String Percolation Approach at RHIC Energies. *Eur. Phys. J. A* **2018**, *54*, 136.
54. Aduszkiewicz, A.; Ali, Y.; Andronov, E.; Antićić, T.; Baatar, B.; Baszczyk, M.; Bhosale, S.; Blondel, A.; Bogomilov, M.; Brandin, A.; et al. Measurements of $\pi^{\pm}$, $K^{\pm}$, p and $\bar{p}$ spectra in proton-proton interactions at 20, 31, 40, 80 and 158 GeV/c with the NA61/SHINE spectrometer at the CERN SPS. *Eur. Phys. J. C* **2017**, *77*, 671.
55. Acharya, A.; Adhikary, H.; Aduszkiewicz, A.; Allison, K.K.; Andronov, E.V.; Antićić, T.; Babkin, V.; Baszczyk, M.; Bhosale, S.; Blondel, A.; et al. Measurements of π^- production in ^{7}Be + ^{9}Be collisions at beam momenta from 19A to 150AGeV/c in the NA61/SHINE experiment at the CERN SPS. *Eur. Phys. J. C* **2020**, *80*, 961. Erratum in *Eur. Phys. J. C* **2021**, *81*, 144. [CrossRef]
56. Acharya, A.; Adhikary, H.; Allison, K.K.; Andronov, E.V.; Antićić, T.; Babkin, V.; Baszczyk, M.; Bhosale, S.; Blondel, A.; Bogomilov, M.; et al. Spectra and mean multiplicities of π^- in central ^{40}Ar+^{45}Sc collisions at 13A, 19A, 30A, 40A, 75A and 150A Ge V/c beam momenta measured by the NA61/SHINE spectrometer at the CERN SPS. *Eur. Phys. J. C* **2021**, *81*, 397,
57. Alt, C.; Anticic, T.; Baatar, B.; Barna, D.; Bartke, J.; Betev, L.; Białkowska, H.; Blume, C.; Boimska, B.; Botje, M.; et al. Pion and kaon production in central Pb + Pb collisions at 20-A and 30-A-GeV: Evidence for the onset of deconfinement. *Phys. Rev. C* **2008**, *77*, 024903.
58. Afanasiev, S.V.; Anticic, T.; Barna, D.; Bartke, J.; Barton, R.A.; Behler, M.; Betev, L.; Białkowska, H.; Billmeier, A.; Blume, C.; et al. Energy dependence of pion and kaon production in central Pb + Pb collisions. *Phys. Rev. C* **2002**, *66*, 054902.
59. Waqas, M.; Peng, G.X.; Ajaz, M.; Khubrani, A.M.; Dawi, E.A.; Khan, M.A.; Tawfik, A. Pseudorapidity dependence of the transverse momentum distribution of charged particles in pp collisions at 0.9, 2.36, and 7 TeV. *Results Phys.* **2022**, *42*, 105989. [CrossRef]
60. Waqas, M.; Peng, G.X.; Ajaz, M.; Wazir, Z.; Ismail, A.A.K.H. Decoupling of non-strange, strange and multi-strange particles from the system in Cu–Cu, Au–Au and Pb–Pb collisions at high energies. *Chin. J. Phys.* **2022**, *77*, 1713–1722.
61. Lao, H.L.; Liu, F.H.; Ma, B.Q. Analyzing Transverse Momentum Spectra of Pions, Kaons and Protons in p–p, p–A and A–A Collisions via the Blast-Wave Model with Fluctuations. *Entropy* **2021**, *23*, 803. [CrossRef] [PubMed]
62. Tawfik, A. Chemical Freeze-Out and Higher Order Multiplicity Moments. *Nucl. Phys. A* **2014**, *922*, 225–236. . 6/j.nuclphysa.2013.12.008. [CrossRef]
63. Tawfik, A. On the Higher Moments of Particle Multiplicity, Chemical Freeze-Out and QCD Critical Endpoint. *Adv. High Energy Phys.* **2013**, *2013*, 574871.
64. Tawfik, A. On the conditions driving the chemical freeze-out. *EPL* **2006**, *75*, 420.
65. Andronic, A.; Braun-Munzinger, P.; Redlich, K.; Stachel, J. Decoding the phase structure of QCD via particle production at high energy. *Nature* **2018**, *561*, 321–330.
66. Sharma, N.; Cleymans, J.; Hippolyte, B.; Paradza, M. A Comparison of p-p, p-Pb, Pb-Pb Collisions in the Thermal Model: Multiplicity Dependence of Thermal Parameters. *Phys. Rev. C* **2019**, *99*, 044914.